10271
NACA TN 3915

TECH LIBRARY KAFB, NM
0067128

NATIONAL ADVISORY COMMITTEE FOR AERONAUTICS

TECHNICAL NOTE 3915

FLIGHT INVESTIGATION OF A ROLL-STABILIZED MISSILE CONFIGURATION AT VARYING ANGLES OF ATTACK AT MACH NUMBERS BETWEEN 0.8 AND 1.79

By Jacob Zarovsky and Robert A. Gardiner

Langley Aeronautical Laboratory
Langley Field, Va.

Washington
January 1957

AFMDC
TECHNICAL LIBRARY
AFL 2811

TECH LIBRARY KAFB, NM

0067128

NATIONAL ADVISORY COMMITTEE FOR AERONAUTICS

TECHNICAL NOTE 3915

FLIGHT INVESTIGATION OF A ROLL-STABILIZED MISSILE CONFIGURATION AT VARYING ANGLES OF ATTACK AT MACH NUMBERS BETWEEN 0.8 AND 1.79[1]

By Jacob Zarovsky and Robert A. Gardiner

SUMMARY

Results are presented of a flight investigation of a rocket-propelled roll-stabilized model incorporating a gyro-actuated control and wing-tip ailerons. The model was disturbed in pitch and roll to determine the effect of these disturbances on the roll-stabilization system.

The flight records indicate that satisfactory roll stabilization may be obtained from the combination of wing-tip ailerons and the gyro-actuated automatic-control system during changes in angle of attack and roll trim at supersonic and transonic speeds. In addition to information on the autopilot performance, longitudinal performance data were determined from the flight records.

INTRODUCTION

The problem of providing roll stabilization for pilotless aircraft is of interest to those engaged in missile research and development work. There is no single solution to the roll stabilization problem that applies to all pilotless aircraft and no one autopilot (or autopilot type) that will provide most economically the desired roll stability in all cases. Factors such as aerodynamic damping and control-surface effectiveness vary with the Mach number and the altitude at which the pilotless aircraft fly, as well as with the various aerodynamic configurations.

Analytical and bench test techniques now available are powerful tools in the hands of the automatic-control-system designer. The proof of the control system, however, still lies in flight tests of the equipment, tests in which the autopilot is subjected to all the vibrations and simultaneous accelerations to be encountered in actual use.

---

[1]Supersedes recently declassified NACA Research Memorandum L50H21 by Jacob Zarovsky and Robert A. Gardiner, 1951.

The purpose of this paper is to present the results of the second flight test of a roll-stabilization system of the no-lag direct-coupled gyro-actuated type used in conjunction with wing-tip ailerons. The first flight test, the results of which are reported in reference 1, demonstrated satisfactory supersonic and transonic roll stabilization of the research missile configuration when disturbed in roll but in essentially zero-lift flight. The second flight test subjected the autopilot and airframe to both rolling and pitching disturbances to determine the effect of normal acceleration and changes in pitch attitude on the autopilot operation. The pitching disturbances also made possible the determination of longitudinal aerodynamic data from the flight record.

SYMBOLS

t	time, sec (zero time for flight records is from time of booster rocket firing)
I_x	moment of inertia about the body center line, slug-ft^2
I_y	moment of inertia about an axis through center of gravity, perpendicular to body center line, and lying in plane of horizontal wings, slug-ft^2
I_z	moment of inertia about an axis through center of gravity, perpendicular to body center line, and lying in plane of vertical wings, slug-ft^2
S	wing area in one plane bounded by extension of leading and trailing edges to center line of model, 4.1 sq ft
c	wing mean aerodynamic chord, 1.77 ft
b	wing span, 3.08 ft
V	velocity, ft/sec
q	dynamic pressure, lb/sq ft, or pitching angular velocity
α	angle of attack, positive when the nose is above the relative wind vector, deg
ϕ	angle of roll, positive in roll to right, deg
$\dot{\phi}$	rolling angular velocity, positive to right, $\frac{d\phi}{dt}$, deg/sec

δ_a total differential aileron angle, positive when trailing edge of right aileron is down, deg

δ_a' average aileron deflection, $\frac{\delta_a}{2}$, deg

L rolling moment, positive to right, ft-lb

C_l rolling-moment coefficient, $\frac{L}{qSb}$

C_{l_p} variation of rolling-moment coefficient with rolling-angular-velocity factor, $\frac{\partial C_l}{\partial \frac{\dot{\phi} b}{2V}}$

$C_{l_{\delta_a'}}$ variation of rolling-moment coefficient with average aileron deflection, $\frac{L_{\delta_a'}}{qSb}$

K control gearing ratio; static value of $\frac{\Delta\delta_a}{\Delta\phi}$

C_m pitching-moment coefficient, $\frac{\text{Pitching moment}}{qSc}$

C_{m_α} variation of pitching-moment coefficient with angle of attack, $\frac{\partial C_m}{\partial \alpha}$

C_{m_q} variation of pitching-moment coefficient with pitching-angular-velocity factor, $\frac{\partial C_m}{\partial \frac{qc}{2V}}$

$C_{m_{\dot{\alpha}}}$ variation of pitching-moment coefficient with rate of change of angle-of-attack factor, $\frac{\partial C_m}{\partial \frac{d\alpha}{dt}\left(\frac{c}{2V}\right)}$

δ_e canard-fin (elevator) deflection, positive when trailing edge is down, deg

$C_{m_{\delta e}}$ variation of pitching-moment coefficient with canard-fin deflection, $\frac{\partial C_m}{\partial \delta_e}$

g acceleration due to gravity, 32.2 ft/sec^2

a_t transverse accelerometer reading, g

a_n normal accelerometer reading, g

C_N normal-force coefficient, $\frac{a_n W}{qS}$

C_{N_α} variation of normal-force coefficient with angle of attack, $\frac{\partial C_N}{\partial \alpha}$

C_L lift coefficient, $\frac{\text{Aerodynamic force normal to flight path}}{qS}$

C_{L_α} variation of lift coefficient with angle of attack, $\frac{\partial C_L}{\partial \alpha}$

$C_{L_{\delta e}}$ variation of lift coefficient with canard-fin deflection, $\frac{\partial C_L}{\partial \delta_e}$

ω frequency, radians/sec

M Mach number

W weight of missile, lb

Subscripts:

L left aileron angle only

R right aileron angle only

trim trim condition

METHODS AND APPARATUS

Model and Instrumentation

The airframe used in the flight test described herein was an all-metal research model of the canard missile type. A sketch of the model is shown in figure 1. Basic model dimensions and measured physical characteristics are shown in table I. Two minor differences may be noted between this model and its predecessor described in reference 1. The cylindrical section of fuselage between the canard fins and wings was lengthened 1 inch to allow for the inclusion of a pneumatic power supply. The wing-tip fences were removed because wind-tunnel tests reported in reference 2 indicate that the fences do not improve the control effectiveness or hinge-moment characteristics of wing-tip control surfaces on a 60° delta wing. Like the model of reference 1, this model utilized wing-tip ailerons as roll-control surfaces. One set of ailerons (called control ailerons) was connected through a mechanical linkage to the autopilot and was used for automatic stabilization. The other set of ailerons was pulsed in a repeating square-wave pattern to provide roll disturbances during the flight. In addition, one set of canard fins was moved to produce pitch disturbances. The other set of canard fins was fixed at zero incidence. The movable canard fins and pulsed ailerons were actuated by pneumatic servomotors through suitable mechanical links. The times at which pulses occurred were determined from the flight record. The pulse amplitudes were measured prior to the flight. Typical control-surface pulse information is presented in figure 2.

The model roll-pulsing system was in operation at take-off and applied programed roll disturbances throughout the flight. The pitch control surfaces were set at 0° deflection prior to take-off and remained in that position until approximately 1 second after the model separated from the booster. At that time the canard-fin pulsing system was activated and programed pitch disturbances continued throughout the remainder of the flight.

Model instrumentation was directed primarily toward evaluation of the quality of roll stabilization. Sufficient information was derived from the flight record to determine some rolling- and pitching-stability derivatives.

The model was equipped with an NACA telemeter. Information telemetered included roll position, control-aileron position, total pressure, transverse acceleration, normal acceleration, angle of attack, aileron and canard-fin pulse indications, and a reference static pressure. The total-pressure and transverse-accelerometer outputs were switched on one telemeter channel, and pulse indications displaced the reference values of the static-pressure and total-pressure records.

The booster used to bring the model up to supersonic speed was made up of two 6,000-pound-thrust, 3-second-duration, solid-propellant rocket motors. An adaptor fitting similar to the one mentioned in reference 1 provided a roll-free model mounting on the front of the booster. A photograph of the model and booster on the launching rack is included as figure 3.

The model was launched at approximately 50° from the horizontal. Radar records were obtained for the initial part of the flight. The telemeter continued to function throughout the flight. Radiosonde records were obtained for use in data reduction.

Autopilot

The automatic-control system consisted of a three-degree-of-freedom (position-sensitive) gyroscope, an electric torque motor, and a mechanical linkage connecting the gyroscope and torque motor to the ailerons. A change in the relative roll position of the model with respect to the gyroscope was transmitted from the gyroscope to the ailerons through a cam attached to the outer gimbal of the gyroscope and cam riders attached to the aileron torque rods.

In operation, this type of autopilot will produce control-surface deflections instantaneously in response to changes in roll attitude of the model. The cut of the cam determines the relationship between the roll angle ϕ and the aileron deflection δ_a. The cam may also determine the maximum control-surface deflection. For the model test reported herein, the cam was designed so that $\delta_a = K\phi$, and a value of 0.6 for K was chosen as a result of preflight calculations reported in reference 1. It must be noted that, because of the sign convention employed, the aileron deflection δ_a in the above equation opposes the roll displacement ϕ. On the basis of the flight-test results reported in reference 1, the maximum δ_a was set at $\pm 15^\circ$ for the model test. Since the cam slope was zero for $\phi = \left|\frac{15}{0.6}\right|$, the model could roll beyond that angle with the aileron deflection constant at $\left|15^\circ\right|$ without disturbing the autopilot if a rolling disturbance large enough to cause such a motion is encountered in flight. The cam slope K of the autopilot installed in this model was measured prior to the flight. The measured value of K is noted in table I.

Hinge moments and friction in the aileron linkage appear as torques at the outer gimbal of the gyroscope, and these torques cause precession of the inner gimbal. Electrical contacts built into the inner gimbal sense the direction of precession and transmit power to operate the electric torque motor. The torque motor then restores to the gyroscope the necessary torque to center the inner gimbal and prevent gimbal lock.

A further description of the autopilot operation appears in reference 1. Figure 4 is a photograph of the autopilot installed in the model.

RESULTS AND DISCUSSION

Portions of the telemeter record showing roll position and left-aileron deflection are reproduced in figures 5 and 6. The records indicate successful roll stabilization throughout the Mach number range of interest (from the maximum Mach number of 1.79 down to a Mach number of 0.8).

The aerodynamic rolling derivatives C_{l_p} and $C_{l_{\delta_a}}$, were determined for the roll disturbance occurring after booster separation and prior to the first canard-fin pulse while the model was in essentially zero-lift flight. These data were used to extend the curves obtained from the zero-lift flight reported in reference 1 to the higher Mach number reached. These derivatives are presented in figure 7. The portion of the record used to determine these derivatives is shown in figure 5.

Figure 6 is a typical portion of the roll record during supersonic flight while the model was disturbed and oscillating in the pitch plane. The irregularity of the motion shown in figure 6 as compared with the motion in figure 5 shows that some disturbance other than the pulsed ailerons is affecting the rolling motion of the model. Aerodynamic coupling between the combined normal and transverse motions and the rolling motion is indicated. Figure 6(c) allows simultaneous examination of the roll record and the normal and transverse acceleration records for a part of the flight. The transverse-acceleration record is discussed later. The normal and transverse accelerations are of reasonably large magnitudes, but the moments affecting the rolling motion that may be ascribed to coupling are small relative to the pulsed-aileron moment. The autopilot and tip-aileron control system is obviously capable of stabilizing the model under more severe conditions of aerodynamic coupling than were encountered in this flight.

Continuing roll disturbances would preclude the use of the single-degree-of-freedom roll equation to describe the rolling motion completely. The method used to determine the aerodynamic rolling derivatives in zero-lift flight was based on an analysis of residual oscillations following a step disturbance and is generally inadequate for the analysis of the more complex motion. The rolling derivatives may not readily be determined for the entire flight since the roll disturbances, whether due to coupling or other causes, are randomly applied and are unknown. However, rolling derivatives were extracted from the roll record by the method used to obtain the derivatives reported in reference 1 for time intervals

during which the pitching motion was approaching steady state. During these intervals the coupling moments were also assumed to approach steady state and may have only a small effect on the values of the derivatives determined by this method. The derivatives determined from the flight record are shown in figure 7. The derivatives presented in reference 1 for zero-lift flight are also shown. Derivatives determined during this flight with lift are identified in figure 7 with the average angle of attack for the appropriate interval.

Angle of roll was determined from the record of control-aileron-position by using the relationship $\delta_a = K\phi$. Figure 8 compares the telemetered angle of roll and that determined from the control-aileron-position record. The information available is insufficient to allow a complete explanation of the difference between the curves shown in the figure. Both the autopilot gyroscope and the telemeter instrument gyroscope were carefully balanced. The instrument gyroscope was a small air-driven gyroscope of the coasting type and was considered to be delicate. The autopilot gyroscope was electrically driven on internal model power and was ruggedly constructed. The autopilot outer gimbal was subjected to torques applied by hinge moments, friction, and the electric torque motor. Both gyroscopes were subjected to linear accelerations of large magnitudes (sometimes approximately 25g in the normal and longitudinal directions). Part of the difference may be attributed to possible telemeter error, which is estimated to be a maximum error of 0.8° for the roll angle and of 0.3° for the telemetered control-aileron position. The maximum inaccuracy of K is estimated to be equivalent to a roll angle of 0.5°. Either or both gyroscope references may have been affected by linear accelerations. Although ground tests have shown no tendency of the autopilot gyroscope to drift under simulated hinge-moment loading, the conditions encountered in flight may have resulted in changes in the reference for the autopilot gyroscope. In spite of the relative drifting of the gyroscopes, the excellent agreement of the phase and the small differences in the magnitudes of the roll angles shown in figure 8 indicate satisfactory autopilot operation, especially in consideration of the simplicity of the autopilot tested.

Aileron Hinge Moments

The hinge moments encountered in this flight were not measured quantitatively; however, the frequency of autopilot-torque-motor operation, as indicated by small but identifiable disturbances in the control-aileron record, showed that the hinge moments encountered in the range of Mach numbers covered by the model flight were small. This result agrees with the hinge-moment information reported in reference 1. Changes in angle of attack experienced in this flight had no apparent effect on the control-moment output required of the autopilot.

Longitudinal Stability

Portions of the normal-acceleration and angle-of-attack telemeter records are shown in figure 9. Sufficient telemetered information was available to determine the more important longitudinal aerodynamic derivatives from the flight record. The methods employed in data reduction may be found in the appendixes of references 3 and 4. In general, two sets of derivatives were obtained: one set for a canard-fin deflection of 2.68° and the other set for a deflection of -4.42°. The individual derivatives determined are discussed subsequently. Results from wind-tunnel tests of this configuration are reported in reference 5, and a summary of free-flight and wind-tunnel investigations of this canard configuration are presented in reference 6.

Aerodynamic derivatives C_{N_α} and C_{L_α}.- The values of C_{N_α} were determined directly from the record. Since model instrumentation did not include a longitudinal accelerometer, C_{L_α} could not be directly determined. The difference between C_{L_α} and C_{N_α} for the angles of attack encountered in this flight was estimated and was found to be negligible. A plot of C_{N_α} as a function of Mach number is shown in figure 10. The values of C_{L_α} presented in reference 3 for another 60° delta-wing canard missile research model are also shown.

Static-stability derivative C_{m_α}.- The static pitching-moment derivative C_{m_α} was determined from the angle-of-attack flight record and is presented as a function of Mach number in figure 11(a). The values of C_{m_α} were found to be appreciably lower for the pulses at $\delta_e = 2.68°$ than for the pulses at $\delta_e = -4.42°$; this difference indicates less stability at lower angles of attack. Wind-tunnel data (ref. 5) also show this trend. The aerodynamic-center location is shown in figure 11(b). The aerodynamic-center location determined for the model flight of reference 3 has been compared with that of the present test. Estimated corrections for differences in the geometric characteristics of the two models result in reasonable agreement between the two flight tests.

The curve of aerodynamic-center location shown in figure 11(b) indicates that the variation of C_{m_α} is dependent primarily on C_{L_α}, since the aerodynamic-center location does not seem to vary with δ_e. Wind-tunnel data of reference 5 indicate that the variations of C_{L_α} for various control-surface deflections are of the same order of magnitude as the variations of C_{L_α} with angle of attack. The nonlinearity of C_{L_α} and C_{m_α} shown by this test may therefore be concluded to result from variations in both angle of attack and canard-fin deflection.

Aerodynamic-damping derivatives $C_{m_q} + C_{m_{\dot{\alpha}}}$.- The values of the damping-in-pitch derivatives $C_{m_q} + C_{m_{\dot{\alpha}}}$ as determined from the angle-of-attack flight record are shown in figure 12. About half the damping of the transient motion is due to these derivatives; the remainder of the damping is chiefly due to C_{L_α}.

Control effectiveness.- For the configuration tested, the lift contributed by the control deflection is very small and may even be negative (see ref. 3) so that the control effectiveness is dependent on the ability of the control surface to trim the model at an angle of attack. From the standpoint of maneuverability and automatic control, a high value of α_{trim}/δ_e is desirable. The factors that cause $C_{L_{\delta e}}$ to be small (reduced lift on the wing due to downwash) contribute to a large pitching moment due to canard-fin (elevator) deflection. The lift on the canard fins is approximately canceled by the loss of lift on the wings so that the pitching moment produced by canard-fin deflection approaches a pure couple and changes very little with movement of the center of gravity. The values of $C_{m_{\delta e}}$ derived from the data depend on the assumption that the ratio α_{trim}/δ_e is constant at a given Mach number for the range of α and δ_e encountered. Because of this assumption, $C_{m_{\delta e}}$ reflects the nonlinearity of C_{m_α}. The variation of α_{trim}/δ_e with Mach number for the flight is shown in figure 13(a), and the values of $C_{m_{\delta e}}$ are shown in figure 13(b).

The aerodynamic-control derivative $C_{L_{\delta e}}$ was not presented because numerical values of the derivative were insignificant. From the standpoint of automatic stabilization and control, the omission of $C_{L_{\delta e}}$ from the motion equations for this canard configuration has no noticeable effect on calculated airframe characteristics. Values of $C_{L_{\delta e}}$ determined for another flight test of a canard model are reported in reference 3.

Nonlinearities.- The flight-test data show that the aerodynamic derivatives for this configuration are somewhat nonlinear. Wind-tunnel data (ref. 5) indicate that C_{m_α} and C_{L_α} are nonlinear. (See points on figs. 10 and 11(a).) The wind-tunnel tests also show that the lift and pitching-moment variations with both angle of attack and canard-fin deflection are nonlinear. No nonlinearities were apparent in the data determined from the flight reported in reference 3. The symmetrical canard-fin pulse of reference 3 and the resultant symmetrical angle-of-attack variations yielded, as would be expected, consistent data and indicated that the derivatives were linear; nonlinearities may be obscured by the symmetrical testing procedure and the methods of data reduction.

The model of reference 3 was not stabilized in roll. The good agreement with the derivatives determined from the flight record of the roll-stabilized model under comparable flight conditions indicates that flight tests of free-to-roll models will yield satisfactory longitudinal data for analysis and design work, provided that reasonable care is exercised in model construction so that rolling velocities are held to low values.

Longitudinal Frequency Response

The longitudinal frequency responses of α/δ_e were determined from the α transients for the δ_e pulses in the Mach number range of interest. These responses will be useful in automatic-stabilization analyses. The method used to determine the frequency responses from the transients is that given in reference 7. Figure 14 shows a typical frequency-response curve. The resonant frequencies (or damped natural frequencies) are plotted in figure 15 at the average Mach numbers for the intervals during which the frequency responses were determined. The resonant-frequency points reflect the nonlinearity of C_{m_α}, which is the aerodynamic spring-constant coefficient of the system in the pitch plane and is the most influential of the derivatives in determining the frequency of the model motion. The resonant frequency is dependent also on the dynamic pressure q. (This effect accounts for the increase in the resonant frequency with increasing Mach number, although the value of C_{m_α} is decreasing.) For this reason any factors which affect q, such as changes in altitude, also affect the resonant frequency.

Transverse Accelerations

The model was not deliberately disturbed in the transverse plane. It was expected that components of acceleration in the plane of pitch disturbances would affect the transverse accelerometer with changes in the roll attitude, since model instrumentation senses motions and accelerations with respect to the model axes. However, the resultant of the normal and transverse acceleration vectors does not rotate in the same manner that the model rotates about its roll axis. Again, aerodynamic coupling is indicated. The effect of the transverse motion on the pitching motion would be small because of the relative magnitudes of the motions. A portion of the transverse-acceleration record appears in figure 9.

Gusts

This flight took place in an overcast immediately preceding a rainstorm. The assumption that gusts were prevalent at the time is a reasonable one. Some abrupt changes in the transverse-acceleration record may be attributed to gusts encountered in flight. Evidence of gusts also appeared in the angle-of-attack and normal-acceleration records, but these disturbances were small in relation to the pitching motion and should have no appreciable effect on derivatives obtained from the record. The effect of gusts on the rolling motion is not known, but it is probable that the primary effect would be the introduction of rolling moments due to aerodynamic coupling.

CONCLUSIONS

Results of a flight test of a roll-stabilization missile configuration at various angles of attack at Mach numbers from 0.8 to 1.79 indicate the following conclusions:

1. The configuration tested was found to be stabilized in roll while flying with varying lift at supersonic and transonic speeds by the use of the gyro-actuated control system and wing-tip ailerons under the conditions encountered in the flight.

2. The tip-aileron and gyro-actuated control combination appears to be capable of stabilizing this model in roll under more severe conditions of aerodynamic coupling than were encountered in this flight.

3. The flight of free-to-roll models will yield satisfactory longitudinal data for analysis and design work, provided that reasonable care is exercised in model construction so that rolling velocities are held to low values.

4. The longitudinal stability derivatives of the configuration tested are somewhat nonlinear.

5. Second-order or aerodynamic coupling effects are of sufficient magnitude to warrant further investigation.

Langley Aeronautical Laboratory,
National Advisory Committee for Aeronautics,
Langley Field, Va., October 22, 1956.

REFERENCES

1. Gardiner, Robert A., and Zarovsky, Jacob: Rocket-Powered Flight Test of a Roll-Stabilized Supersonic Missile Configuration. NACA RM L9K01a, 1950.

2. Conner, D. William, and May, Ellery B., Jr.: Control Effectiveness Load and Hinge-Moment Characteristics of a Tip Control Surface on a Delta Wing at a Mach Number of 1.9. NACA RM L9H05, 1949.

3. Niewald, Roy J., and Moul, Martin T.: The Longitudinal Stability, Control Effectiveness, and Control Hinge-Moment Characteristics Obtained From a Flight Investigation of a Canard Missile Configuration at Transonic and Supersonic Speeds. NACA RM L50I27, 1950.

4. Gillis, Clarence L., Peck, Robert F., and Vitale, A. James: Preliminary Results From a Free-Flight Investigation at Transonic and Supersonic Speeds of the Longitudinal Stability and Control Characteristics of an Airplane Configuration With a Thin Straight Wing of Aspect Ratio 3. NACA RM L9K25a, 1950.

5. Grigsby, Carl E.: Investigation of a Canard Missile Configuration (NACA RM-4) in the Langley 9-Inch Supersonic Tunnel at Mach Numbers of 1.62 and 1.93. NACA RM L54E20, 1954.

6. Curfman, Howard J., Jr., and Grigsby, Carl E.: Longitudinal Stability and Control Characteristics of a Canard Missile Configuration for Mach Numbers From 1.1 to 1.93 As Determined From Free-Flight and Wind-Tunnel Investigations. NACA RM L52F06, 1952.

7. Seamans, Robert C., Jr., Bromberg, Benjamin G., and Payne, L. E.: Application of the Performance Operator to Aircraft Automatic Control. Jour. Aero. Sci., vol. 15, no. 9, Sept. 1948, pp. 535-555.

TABLE I

MEASURED MODEL INFORMATION

Model weight, lb	162.5
Moments of inertia:	
I_x, slug-ft^2	0.77
I_y, slug-ft^2	31.3
I_z, slug-ft^2	31.3
Control gearing ratio, K	0.62
Control-aileron no-load maximum deflections:	
δ_{a_L}	7.5° to -7.3°
δ_{a_R}	7.6° to -7.3°
Pulsed-aileron total deflection, δ_a	4.1° to -3.75°
Canard-fin deflections, δ_e	0° to -4.42° to 2.68°
Model dimensions:	
Overall length, in.	130.375
Body diameter, in.	8.0
Wing span, in.	37.0
Total wing area in one plane, sq ft	4.1
Canard-fin span, in.	17.667
[1]Wing trailing-edge location, station, in.	103.0
[1]Canard-fin trailing-edge location, station, in.	39.125
Wing maximum thickness, in.	0.75
Canard-fin maximum thickness, in.	0.25
[1]Center-of-gravity location, station, in.	73.53
Wing mean aerodynamic chord, ft	1.776
[2]Aileron dimensions, per aileron:	
Root chord, in.	8.372
Span, in.	4.833
Maximum thickness, in.	0.25

[1]Station is measured along the length of the body from the point of the model nose contour.

[2]Aileron and canard-fin plan forms are identical. Aileron section is double wedge. Wing and canard fins are flat plates with beveled leading and trailing edges.

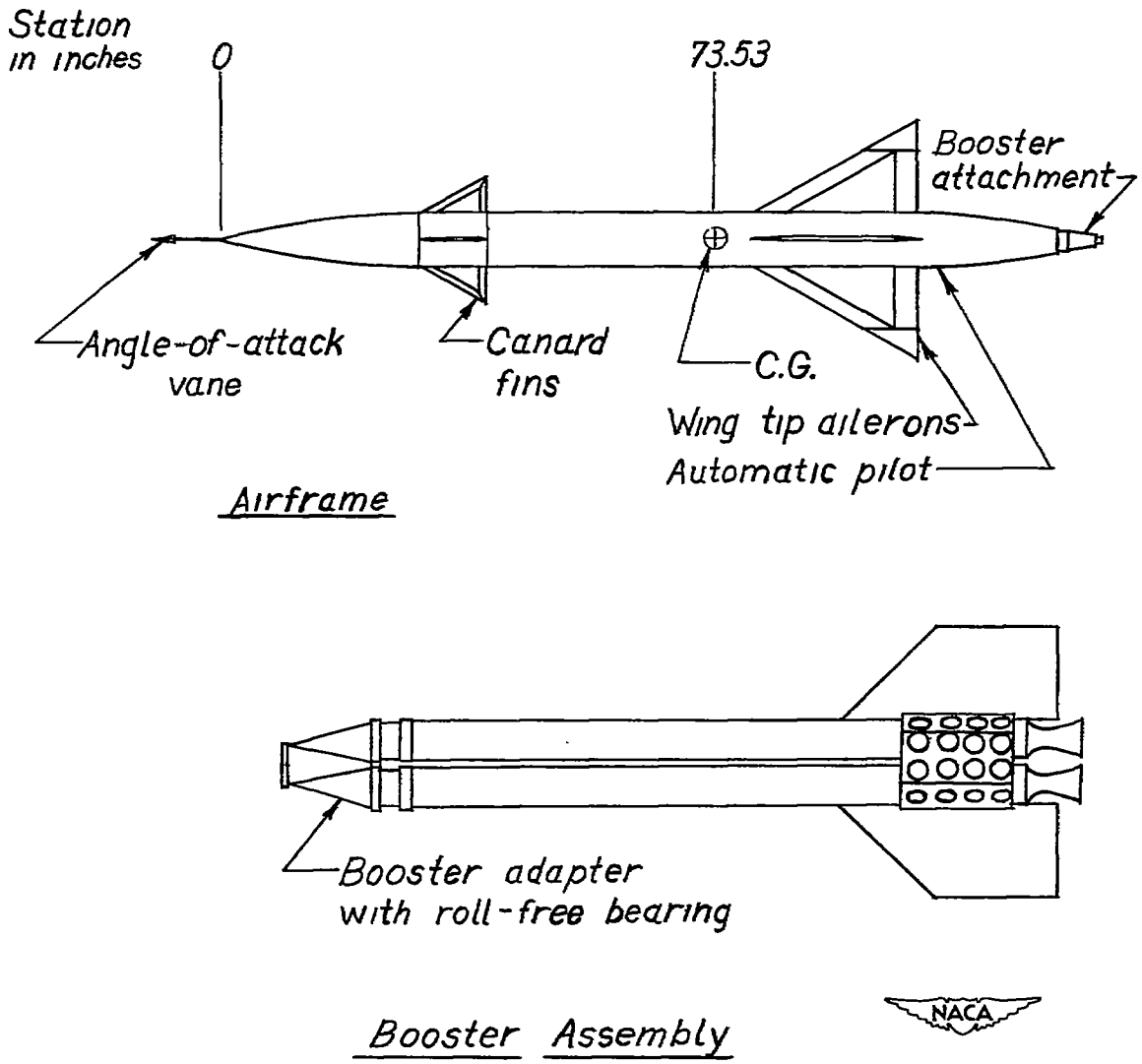

Figure 1.- Sketch of supersonic missile research model and booster assembly.

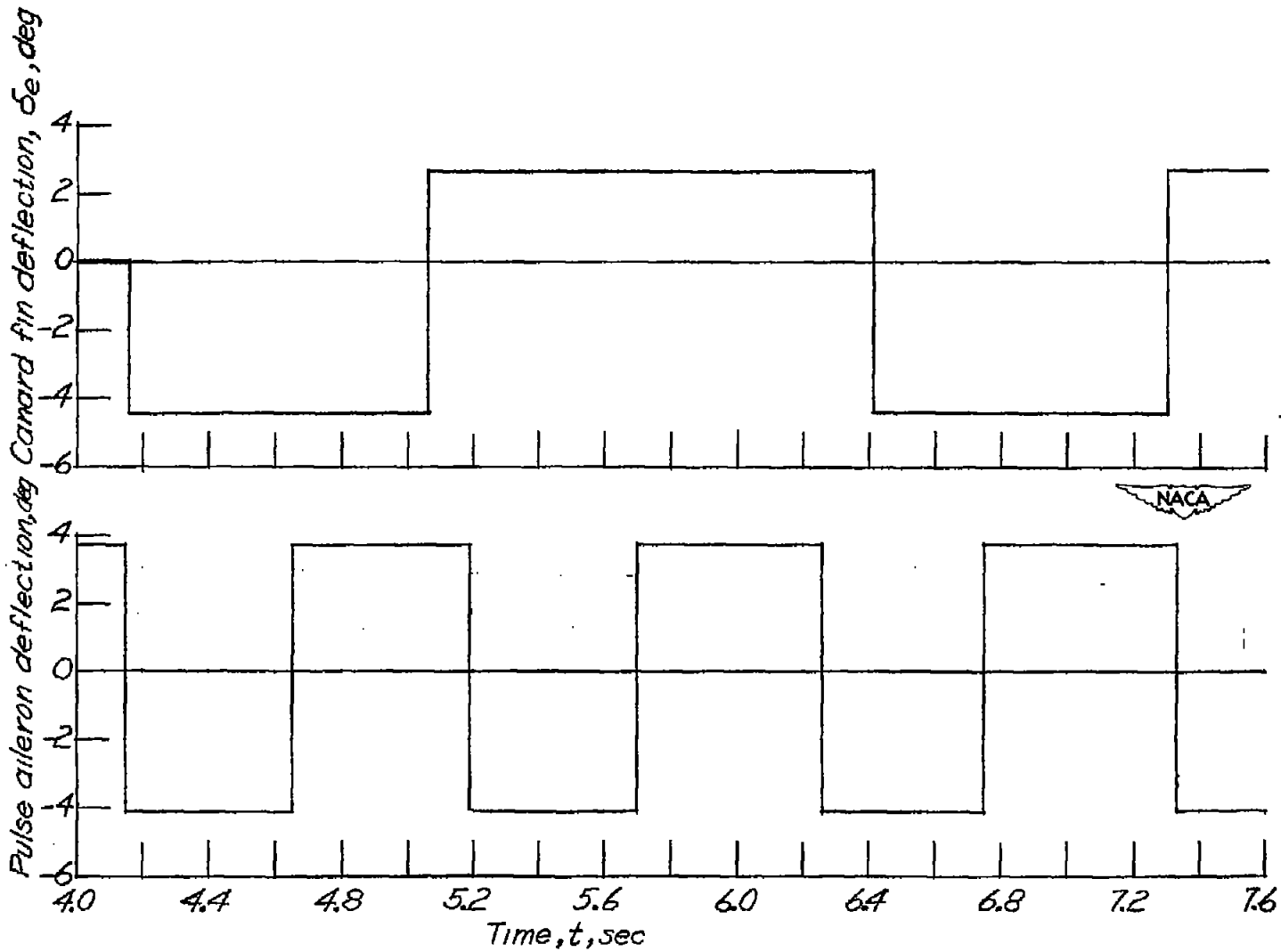

Figure 2.- Disturbing aileron and canard-fin pulse patterns for a portion of flight as determined from the flight record and from preflight measurements of amplitudes.

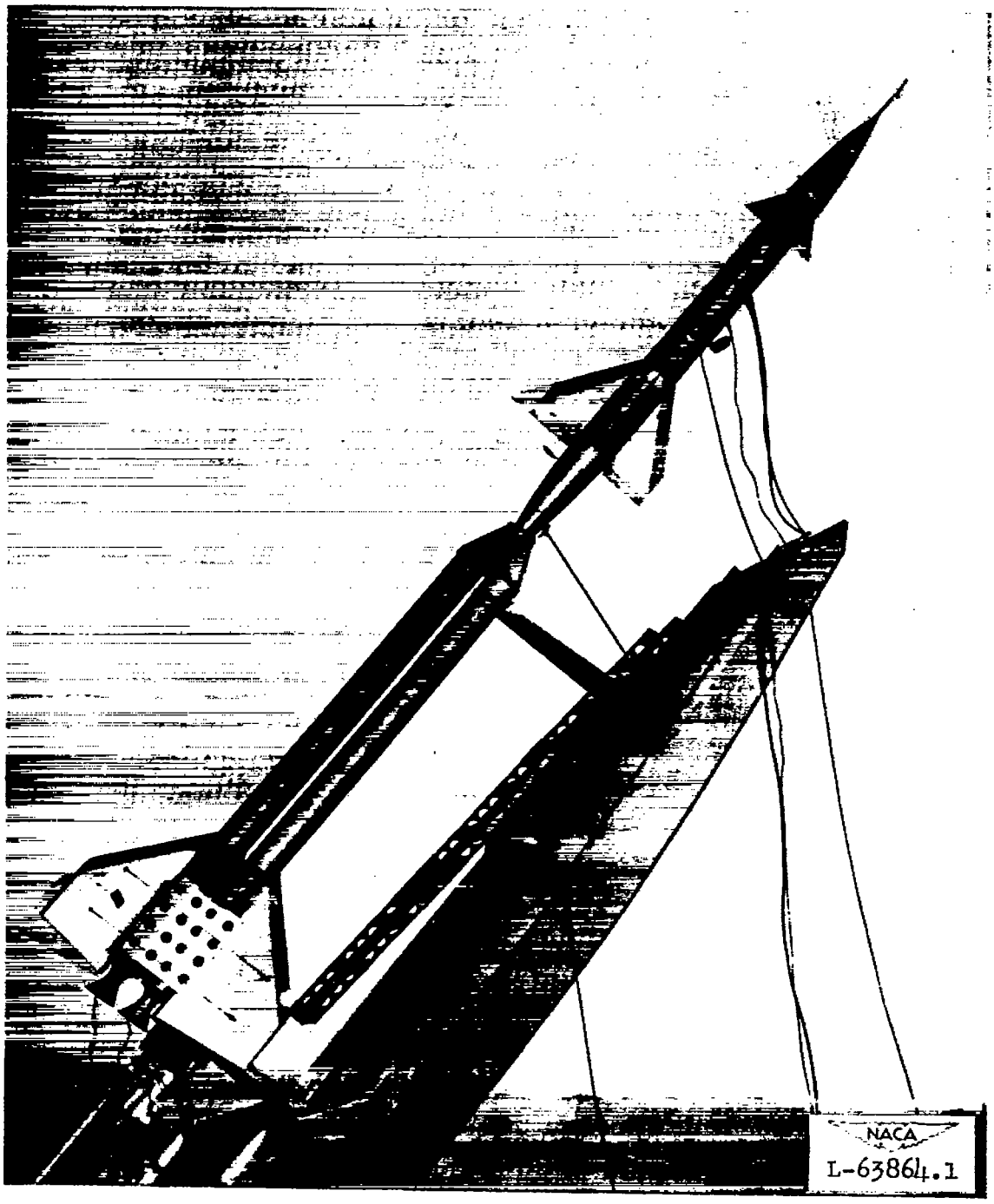

Figure 3.- Photograph of the model on the launcher.

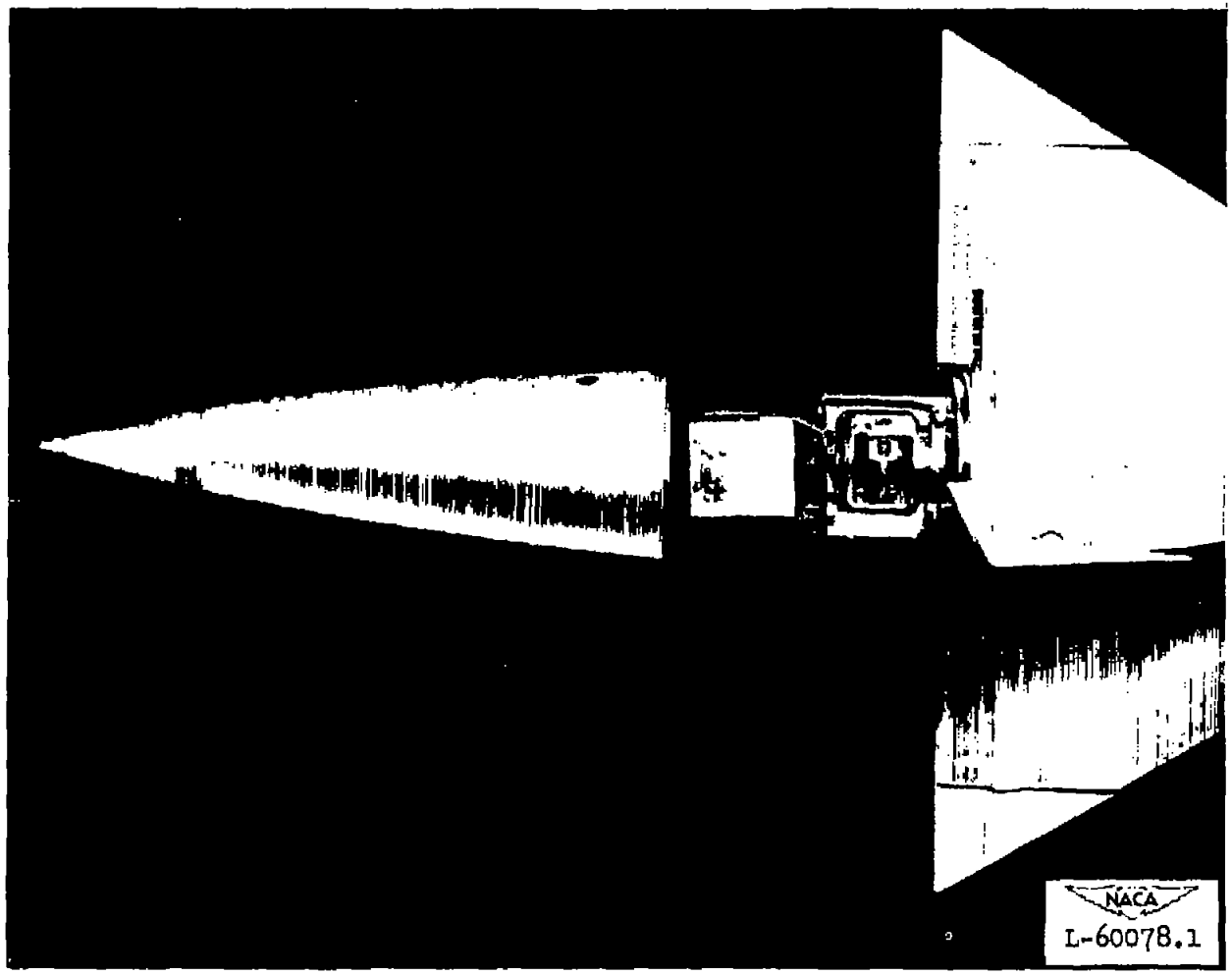

Figure 4.- Photograph of the autopilot installed in the model showing control (horizontal wing) and disturbing (vertical wing) wing-tip ailerons.

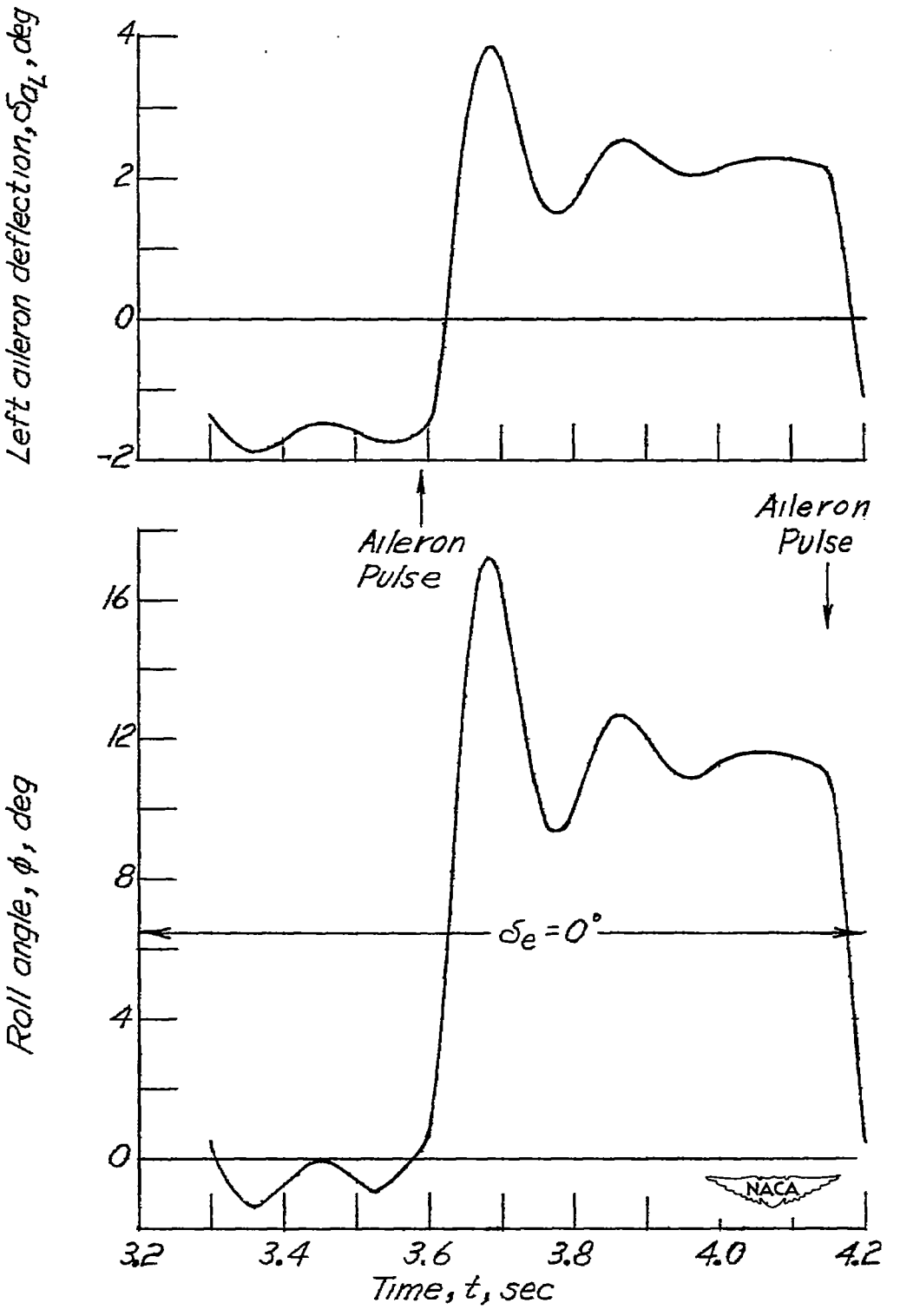

Figure 5.- Portion of roll position and left-aileron-position telemeter records during zero-lift flight.

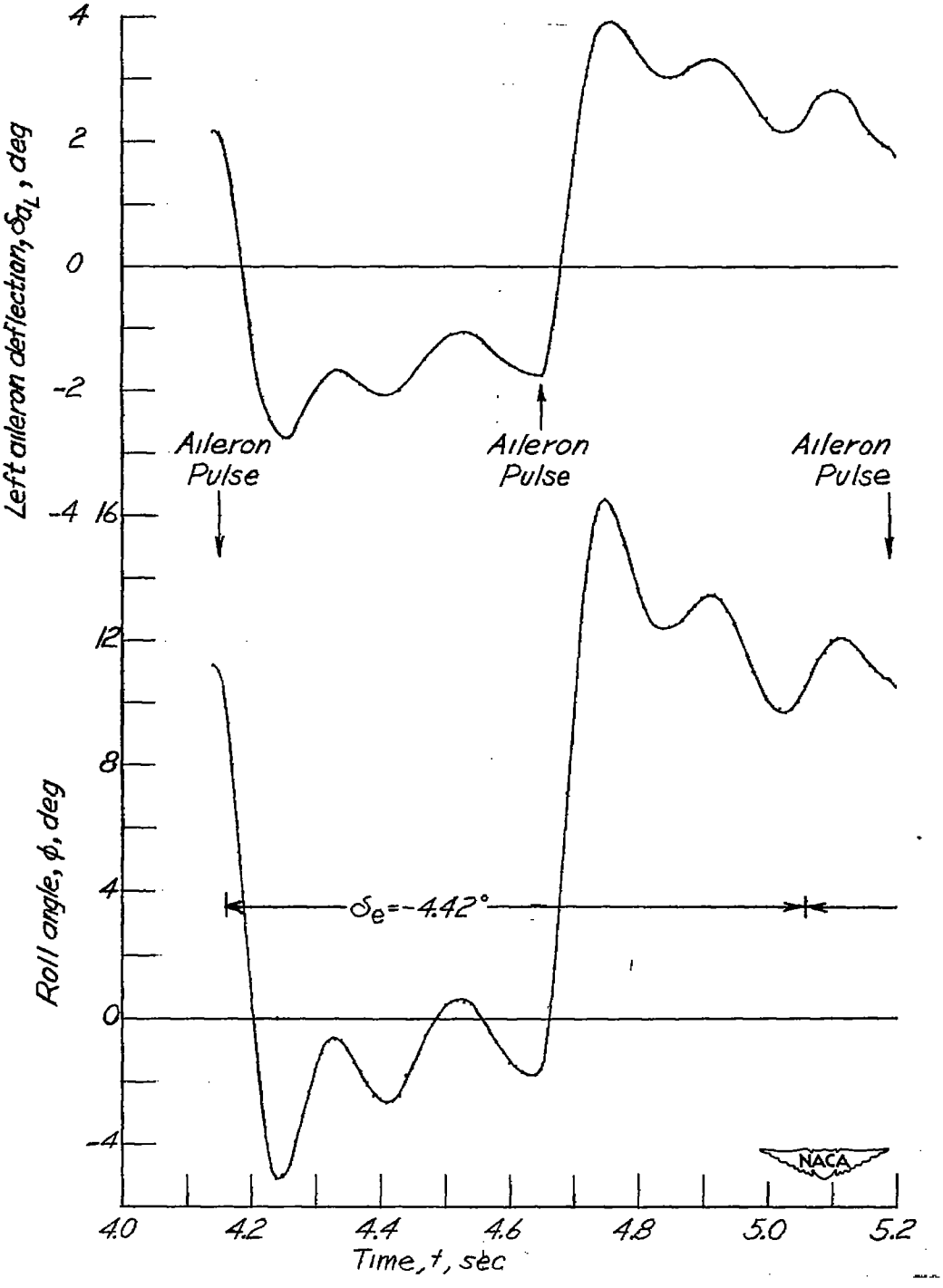

(a) Roll position and left-aileron position. Flight time from 4.0 to 5.2 seconds.

Figure 6.- Typical portions of telemeter record showing information on model rolling motion at varying angles of attack.

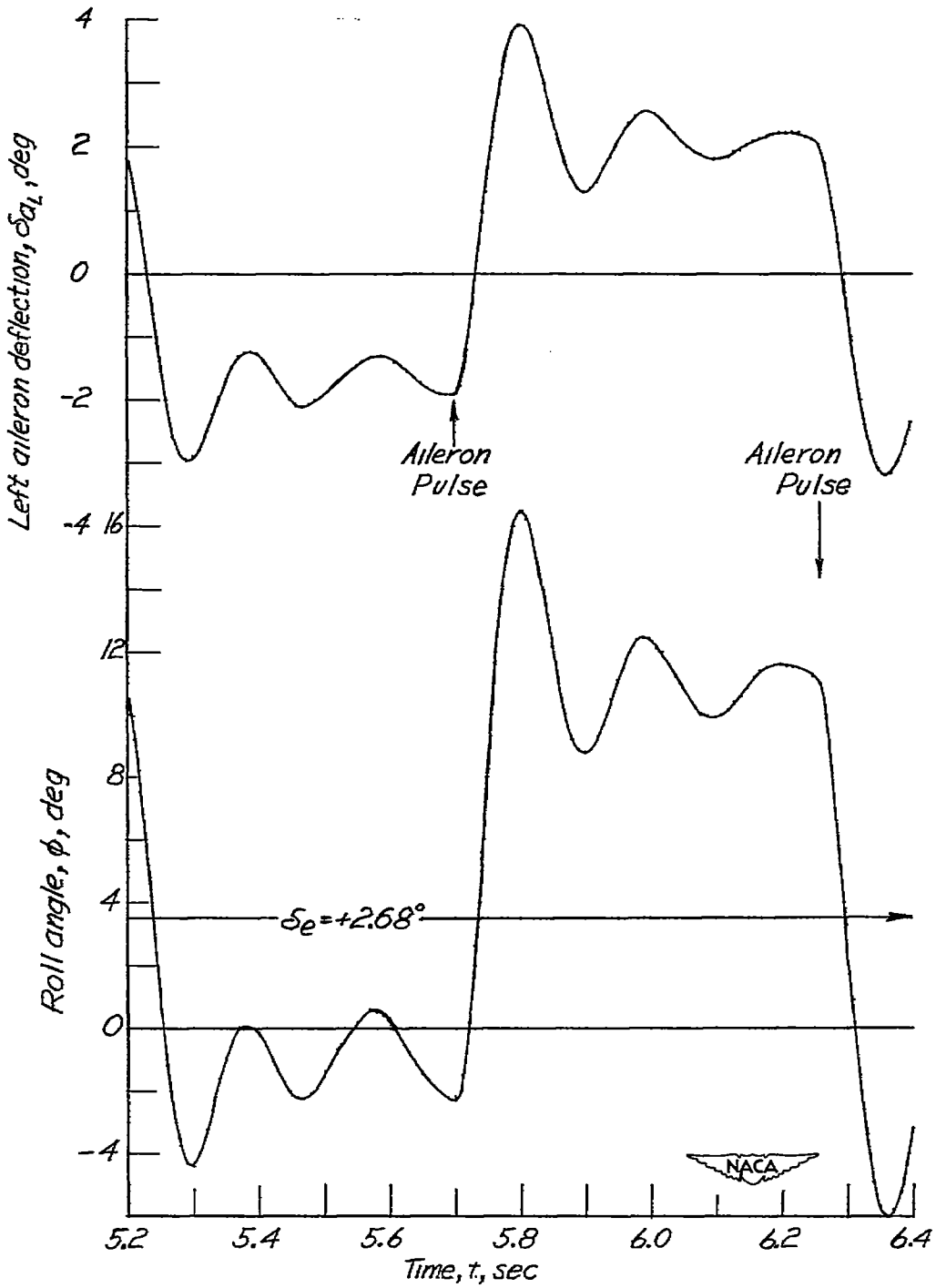

(b) Roll position and left-aileron position. Flight time from 5.2 to 6.4 seconds.

Figure 6.- Continued.

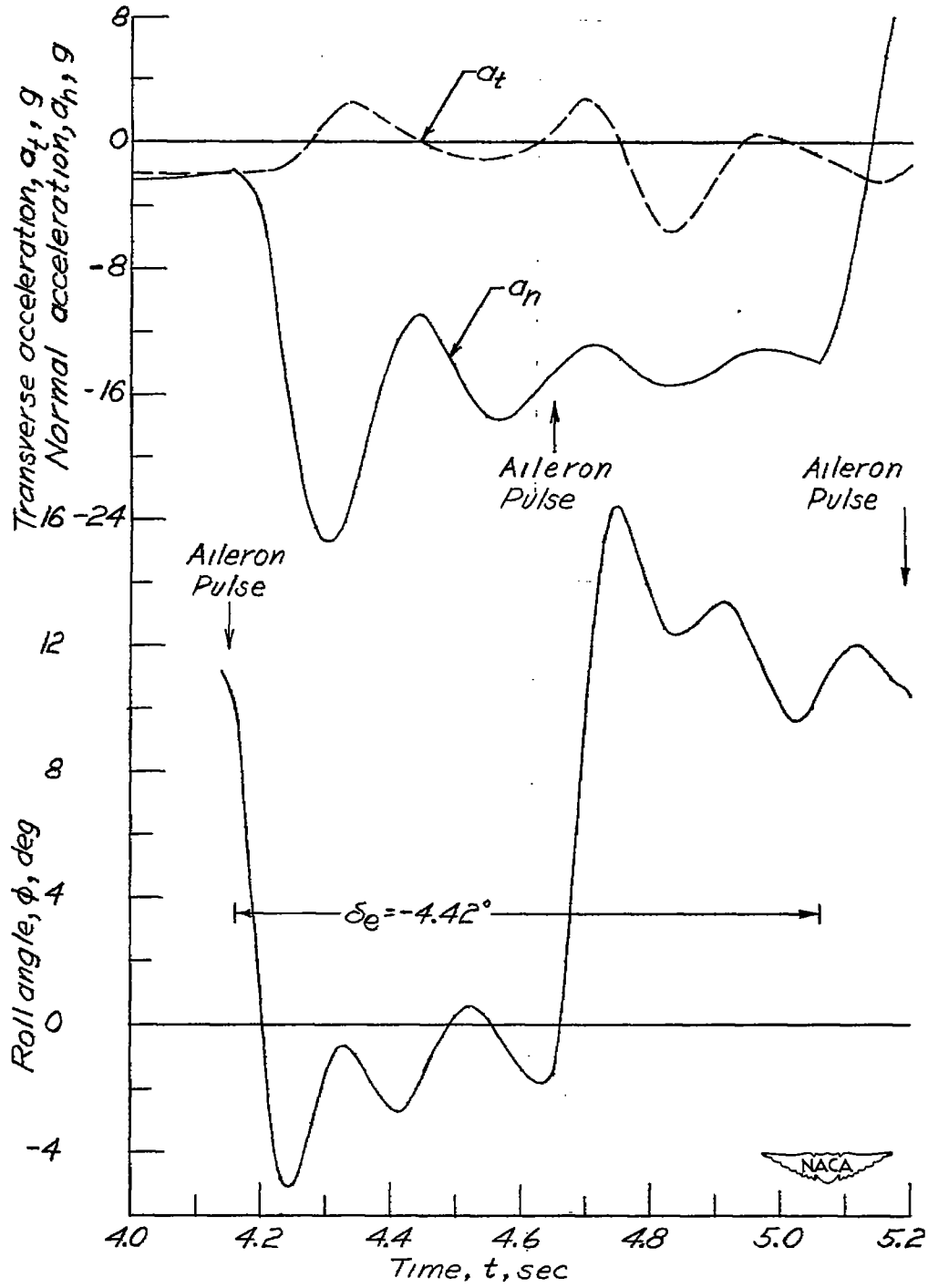

(c) Roll position and normal and transverse accelerations from 4.0 to 5.2 seconds flight time.

Figure 6.- Concluded.

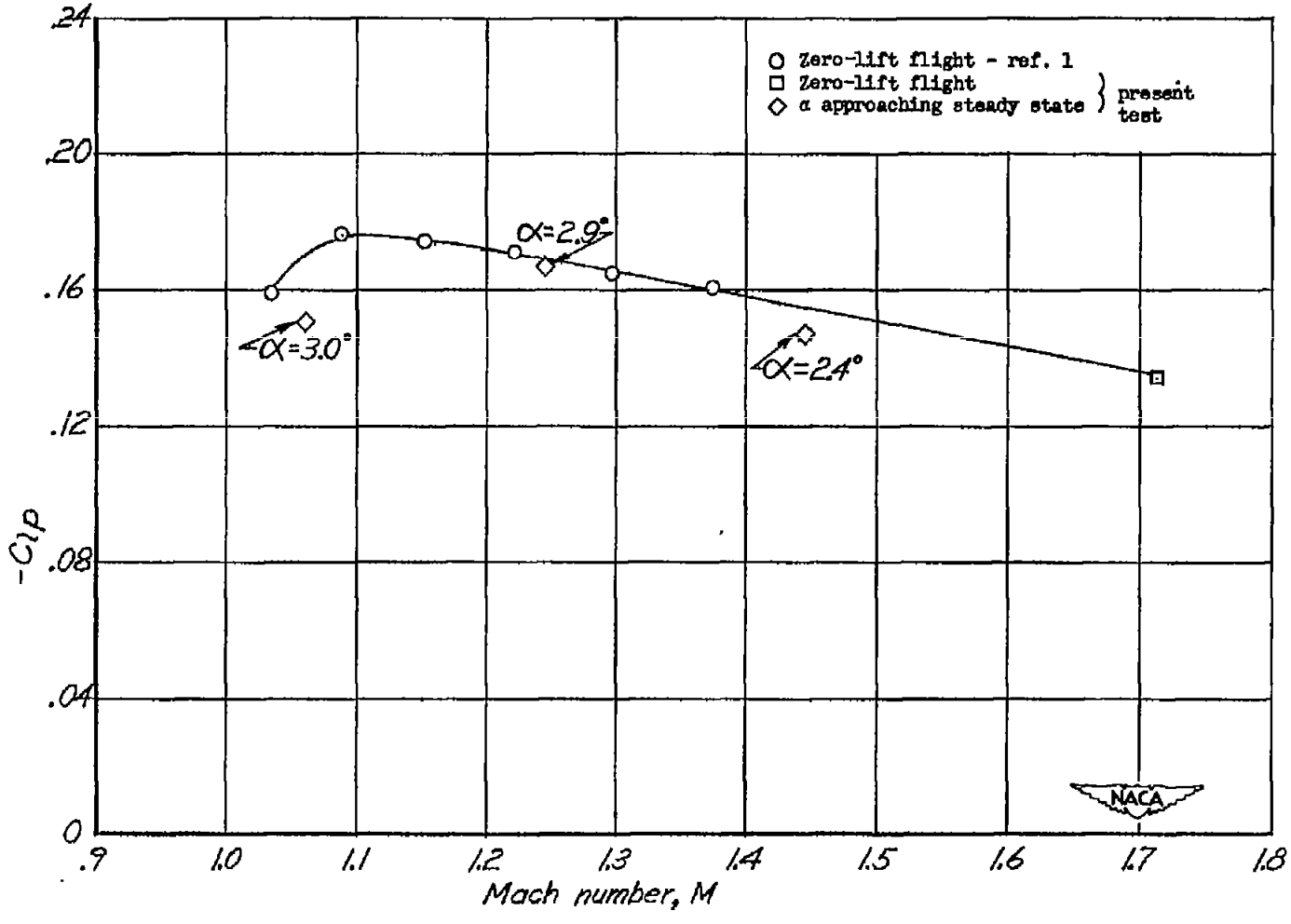

(a) Damping-in-roll parameter C_{l_p}.

Figure 7.- Aerodynamic roll derivatives for the missile model determined from the flight records.

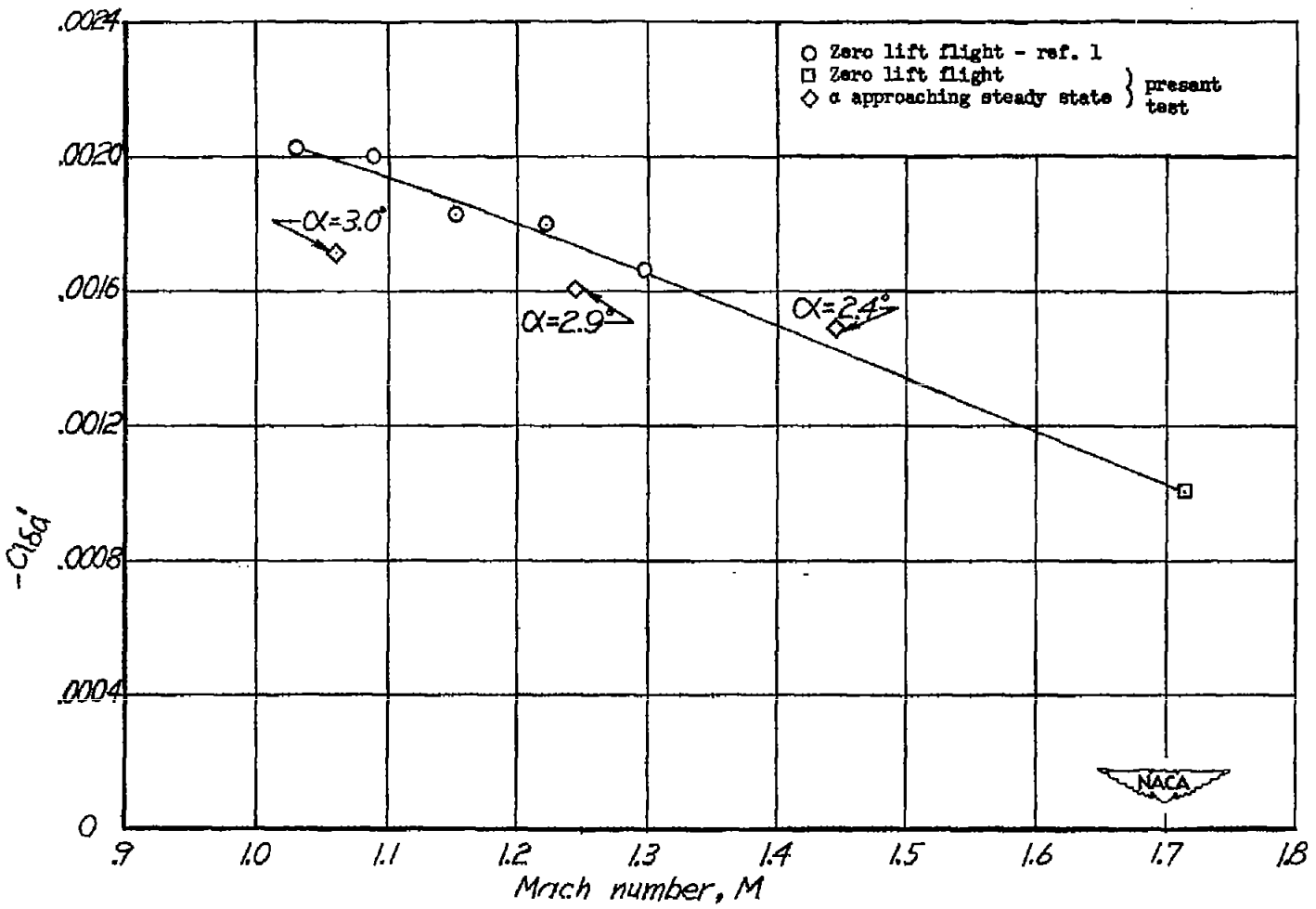

(b) Aileron-effectiveness derivative $C_{l_{\delta a}}'$.

Figure 7.- Concluded.

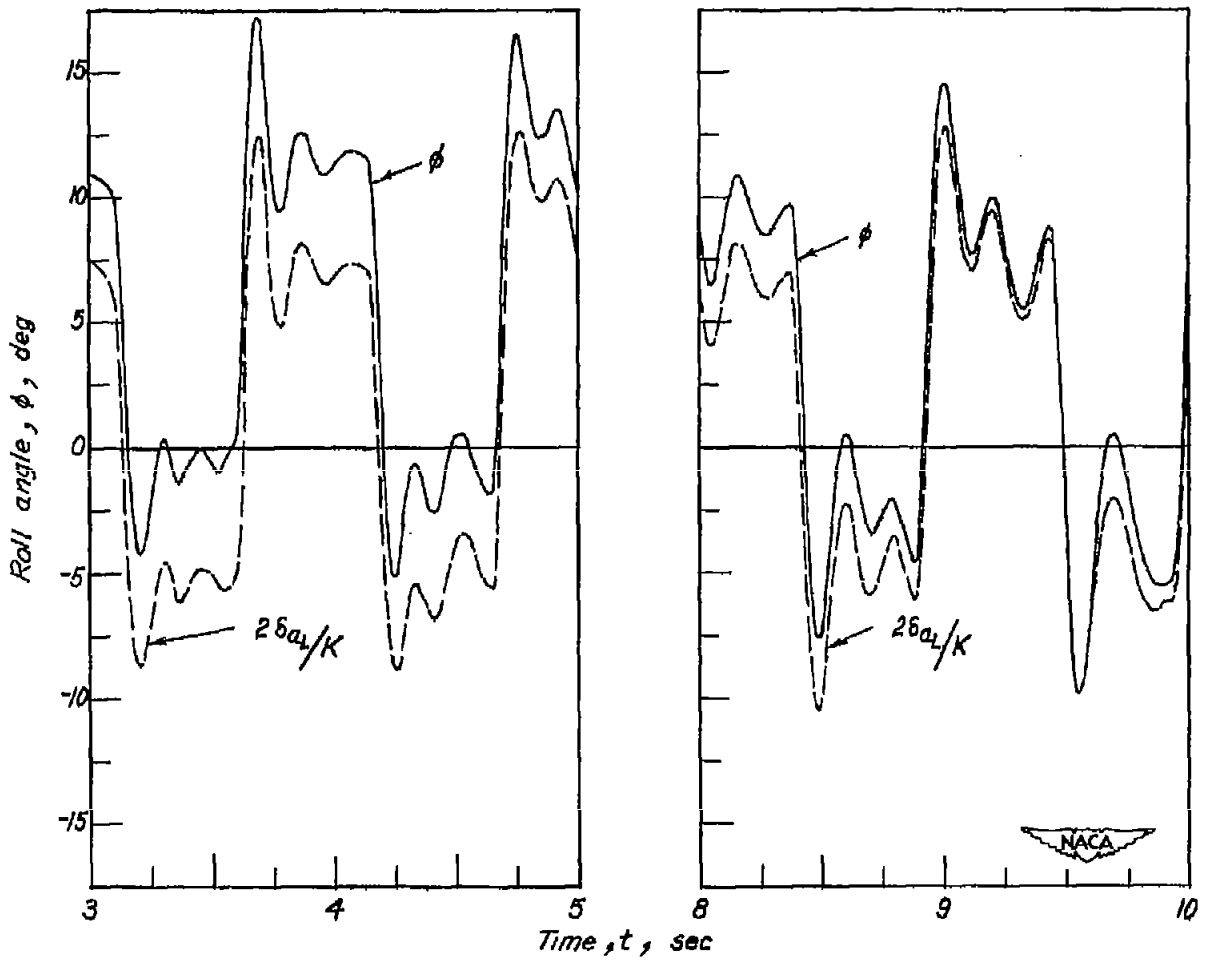

(a) Time from 3.0 to 5.0 seconds and 8.0 to 10.0 seconds.

Figure 8.- Comparison of roll position determined from telemeter roll gyroscope with that calculated from aileron position using the relationship $\delta_a = K\phi$.

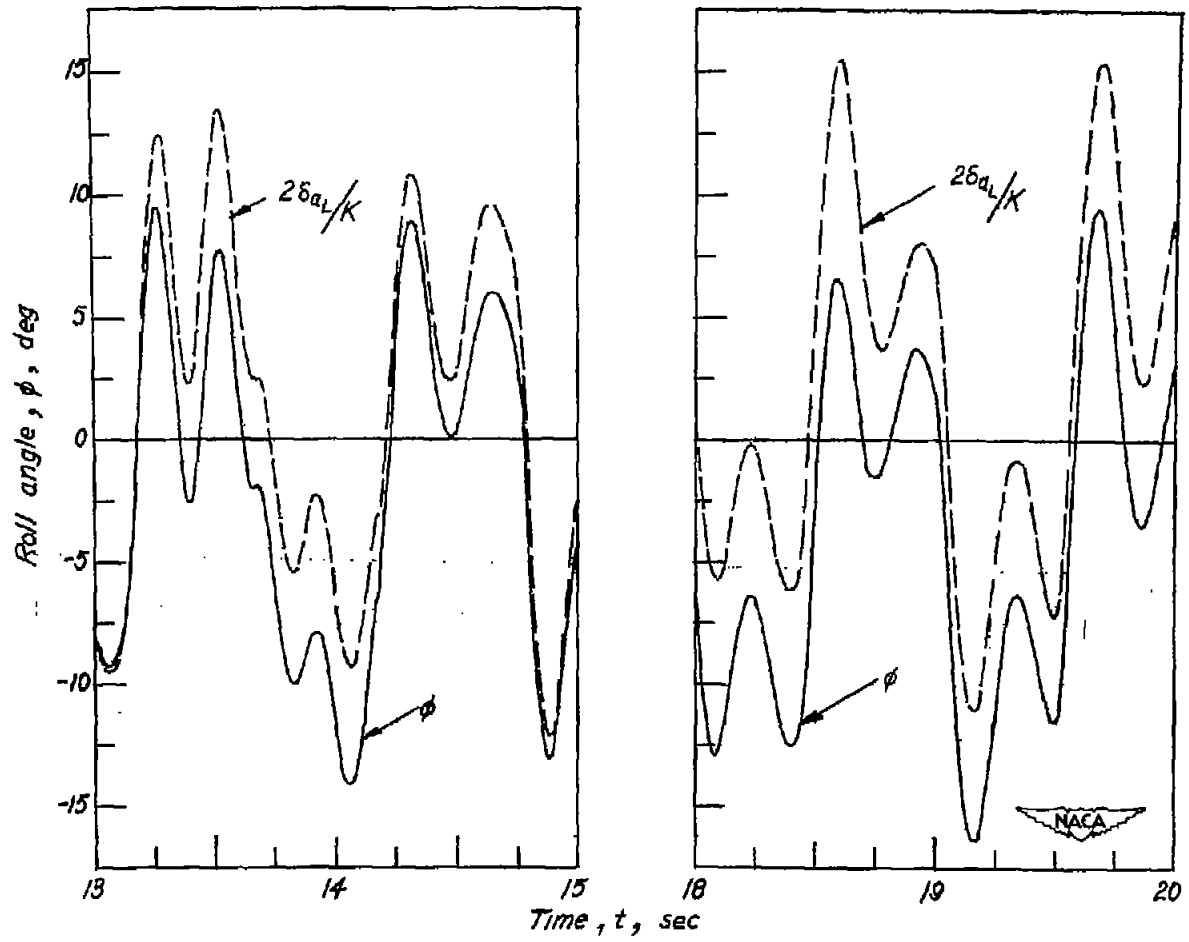

(b) Time from 13.0 to 15.0 seconds and 18.0 to 20.0 seconds.

Figure 8.- Concluded.

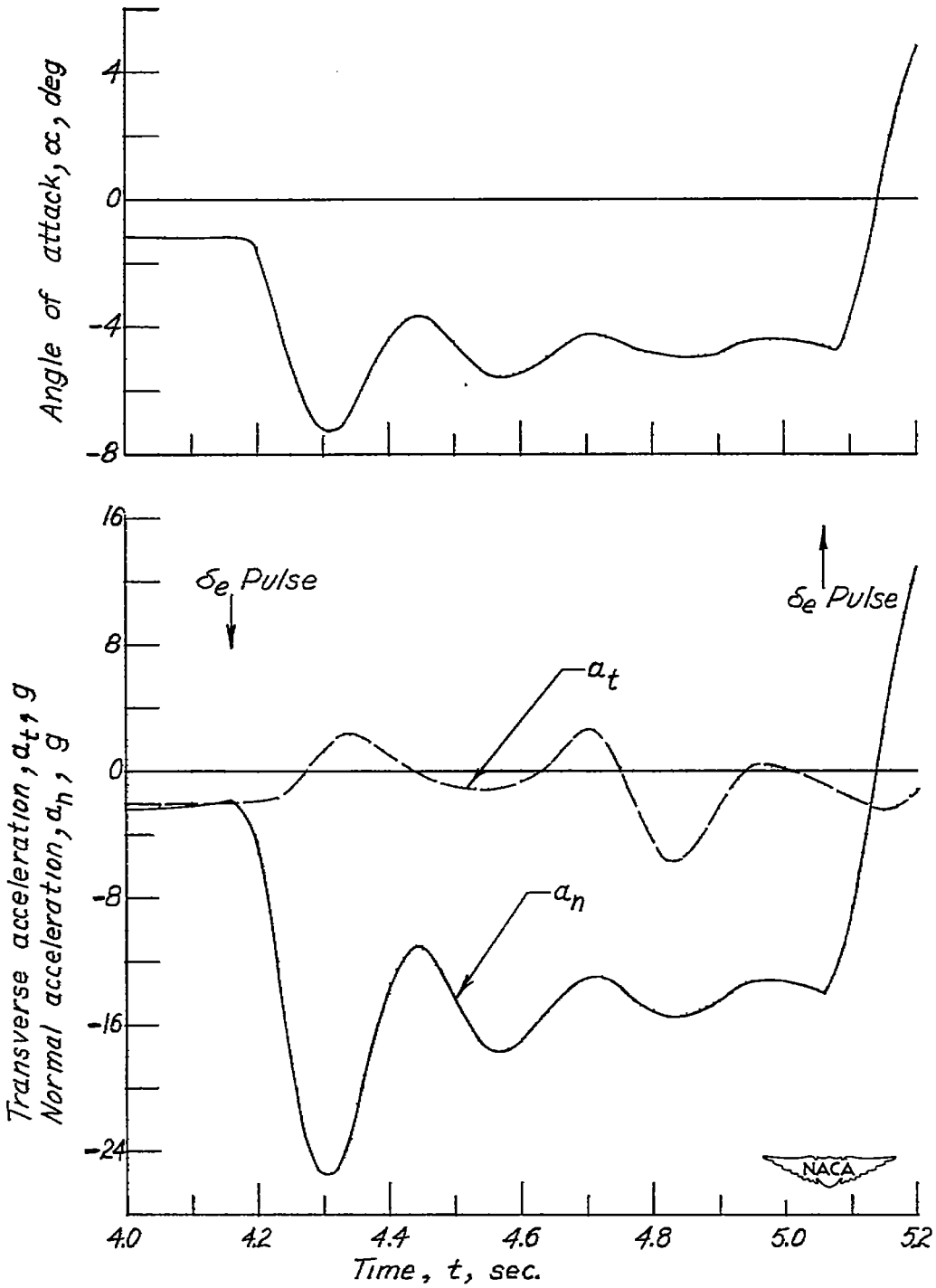

(a) Flight time from 4.0 to 5.2 seconds.

Figure 9.- Typical portion of angle of attack, normal acceleration and transverse acceleration telemeter records during supersonic flight.

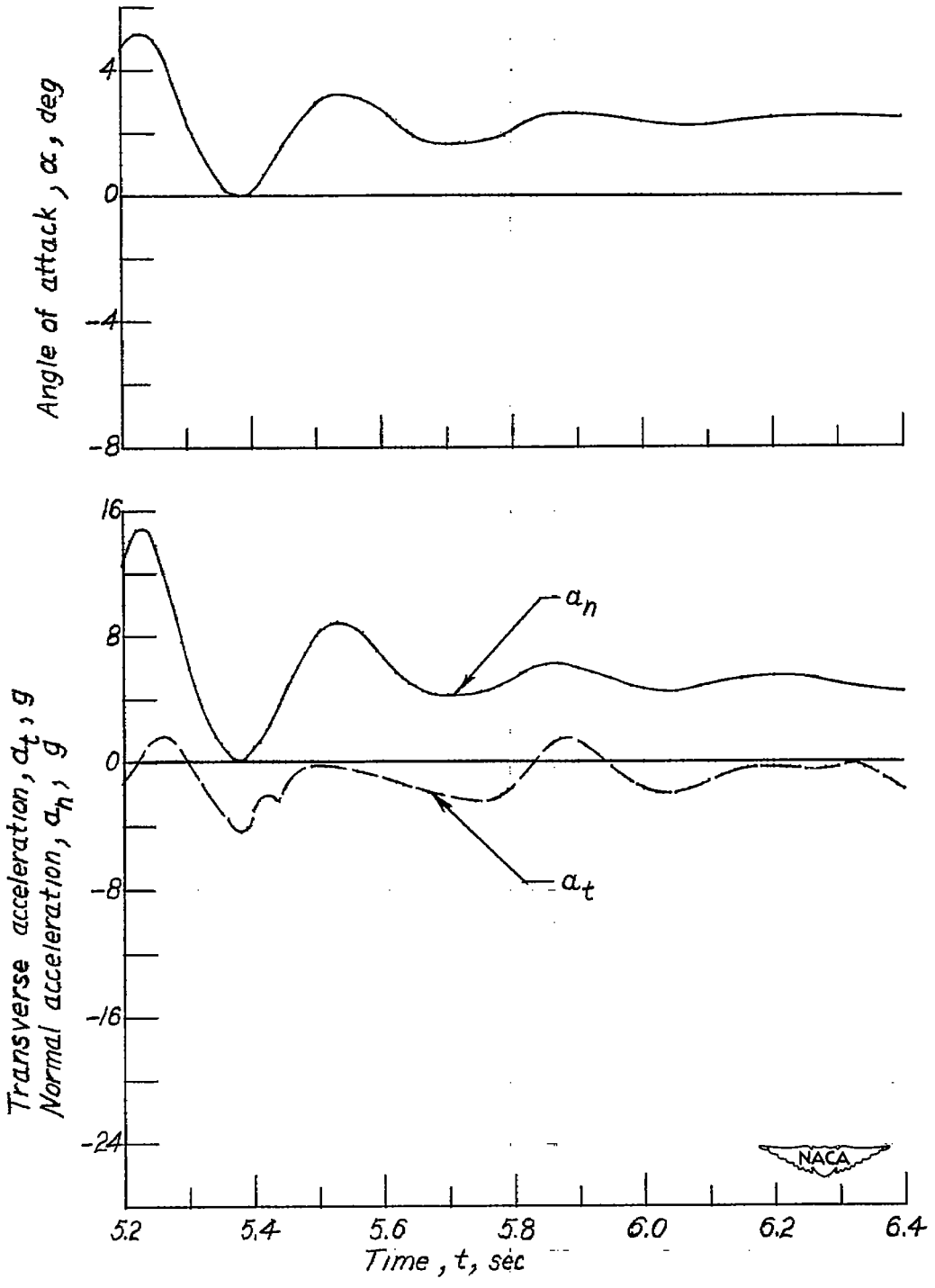

(b) Flight time from 5.2 to 6.4 seconds.

Figure 9.- Concluded.

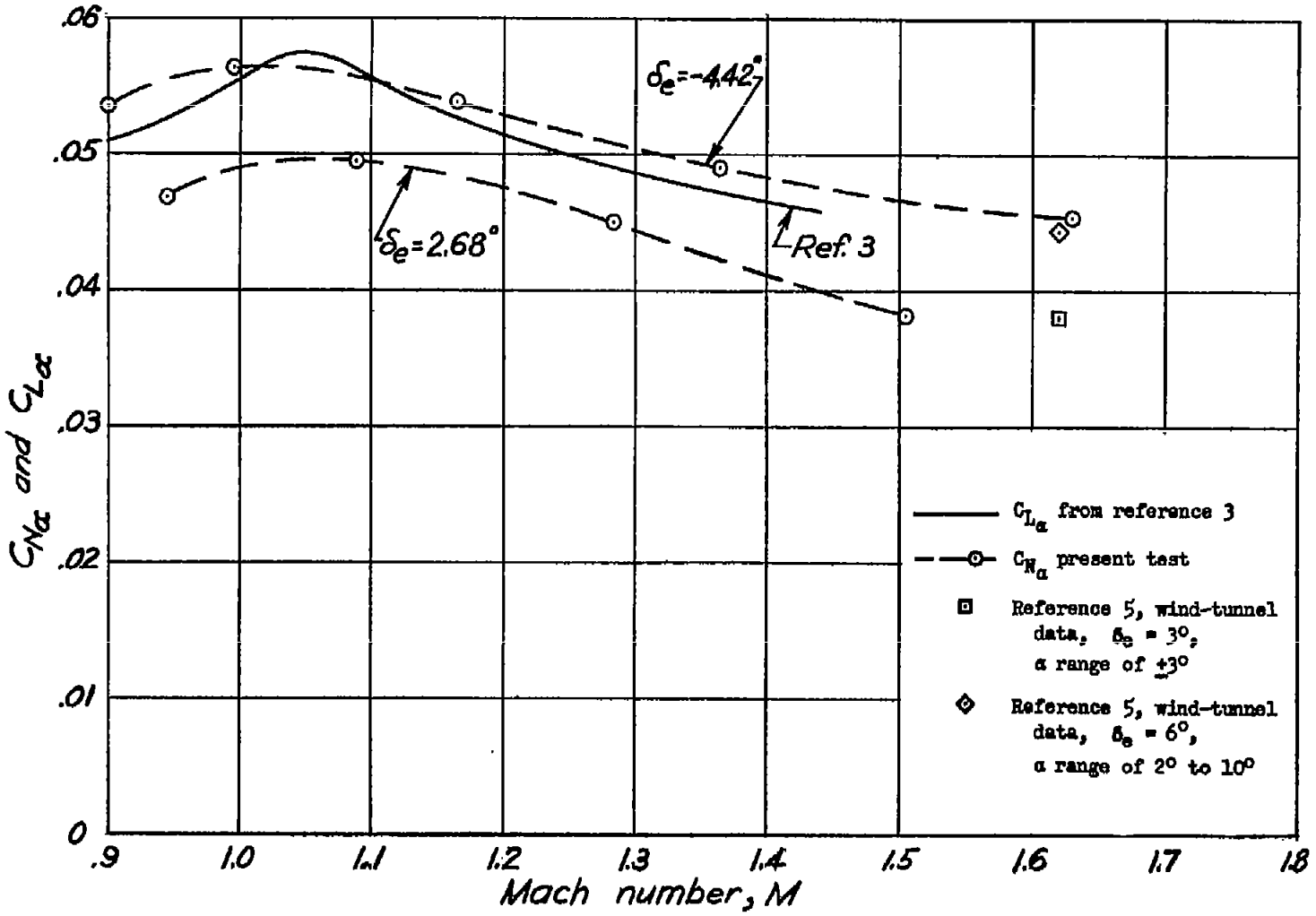

Figure 10.- Normal-force derivative C_{N_α} as determined from the flight records. Data from wind-tunnel and flight tests of a comparable model are shown for comparison.

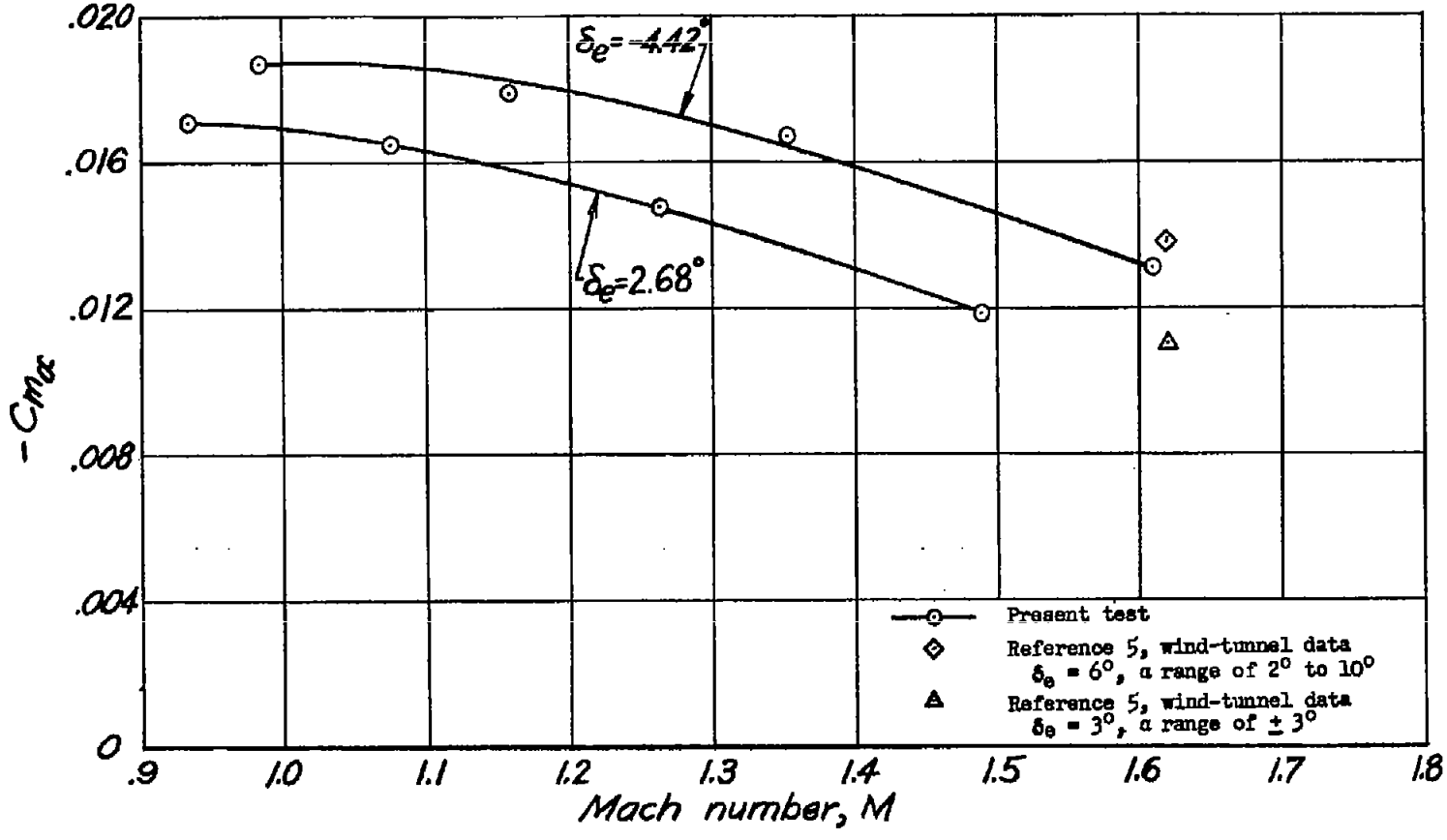

(a) Static pitching-moment derivative C_{m_α}.

Figure 11.- Model static longitudinal-stability data determined from the flight record.

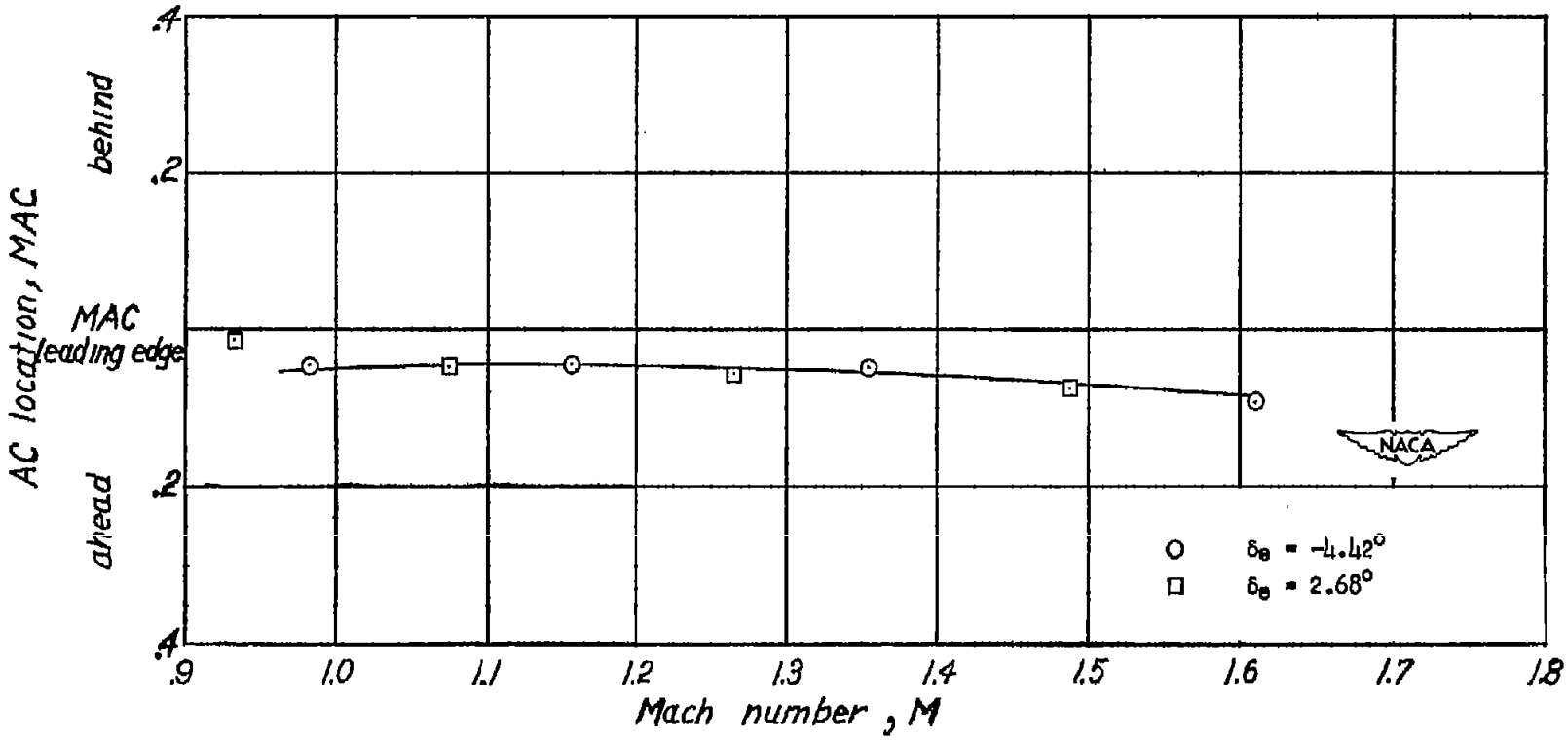

(b) Aerodynamic-center location.

Figure 11.- Concluded.

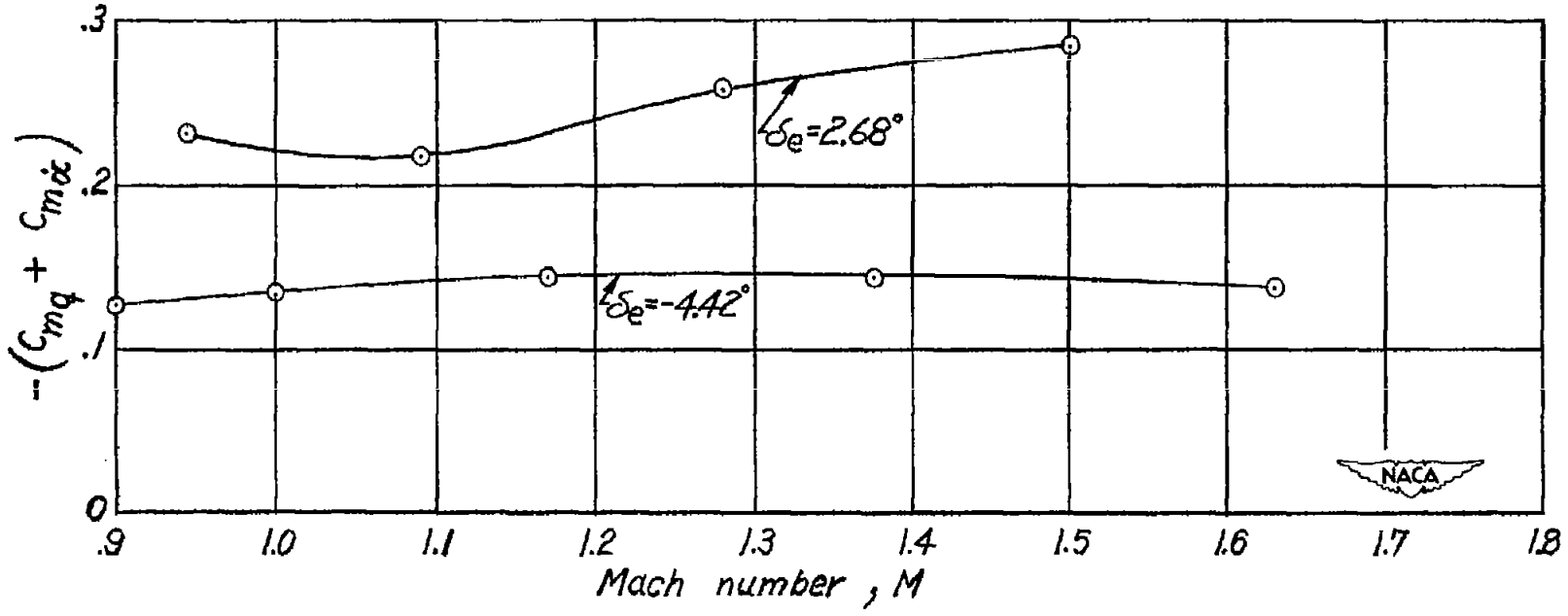

Figure 12.- Aerodynamic damping derivatives $C_{m_q} + C_{m_{\dot{\alpha}}}$ as determined from the flight record.

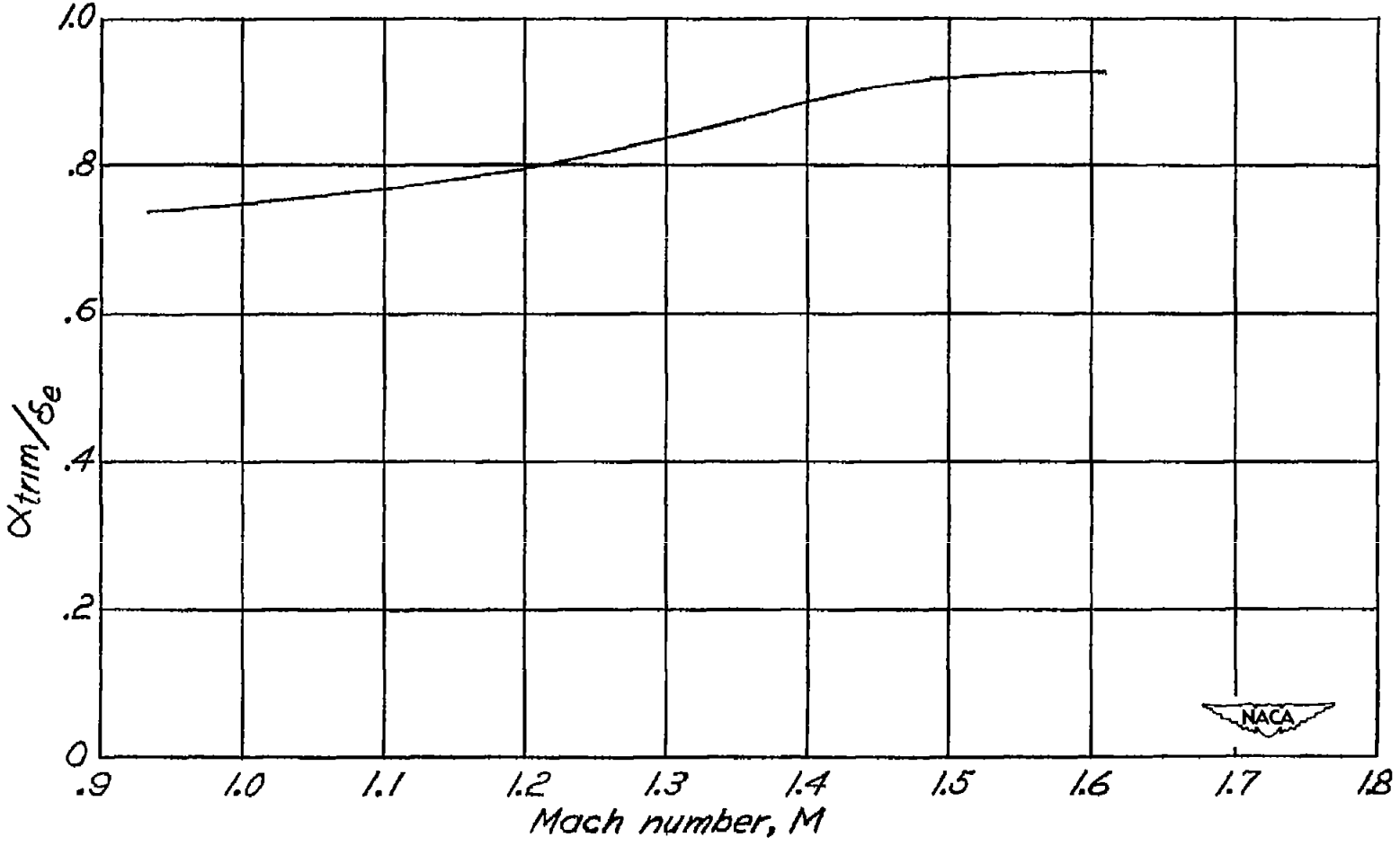

(a) Variation of α_{trim}/δ_e with Mach number.

Figure 13.- Canard-fin (elevator) control-surface effectiveness as determined from the flight record.

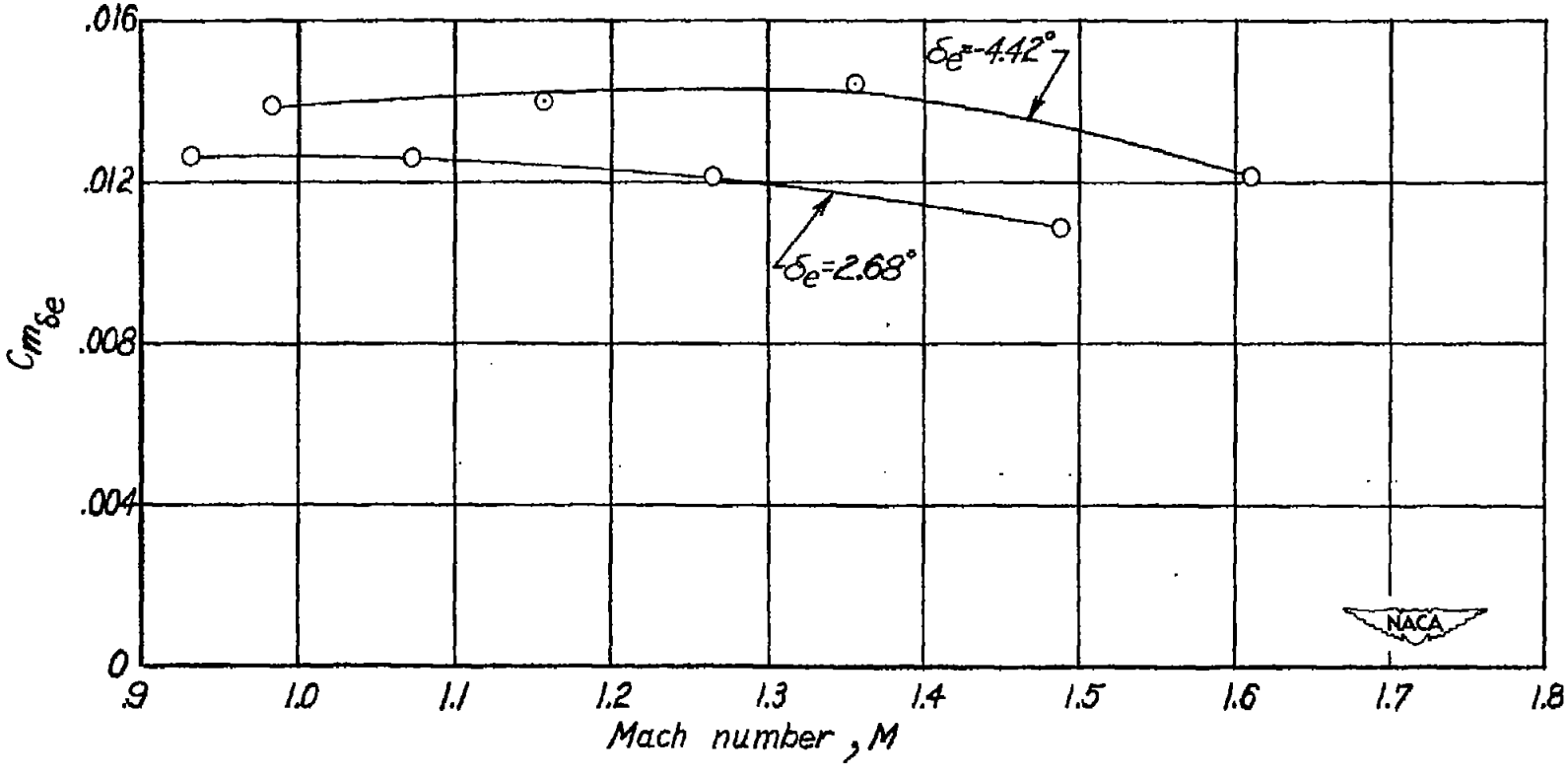

(b) Variation of aerodynamic derivative $C_{m_{\delta_e}}$ with Mach number.

Figure 13.- Concluded.

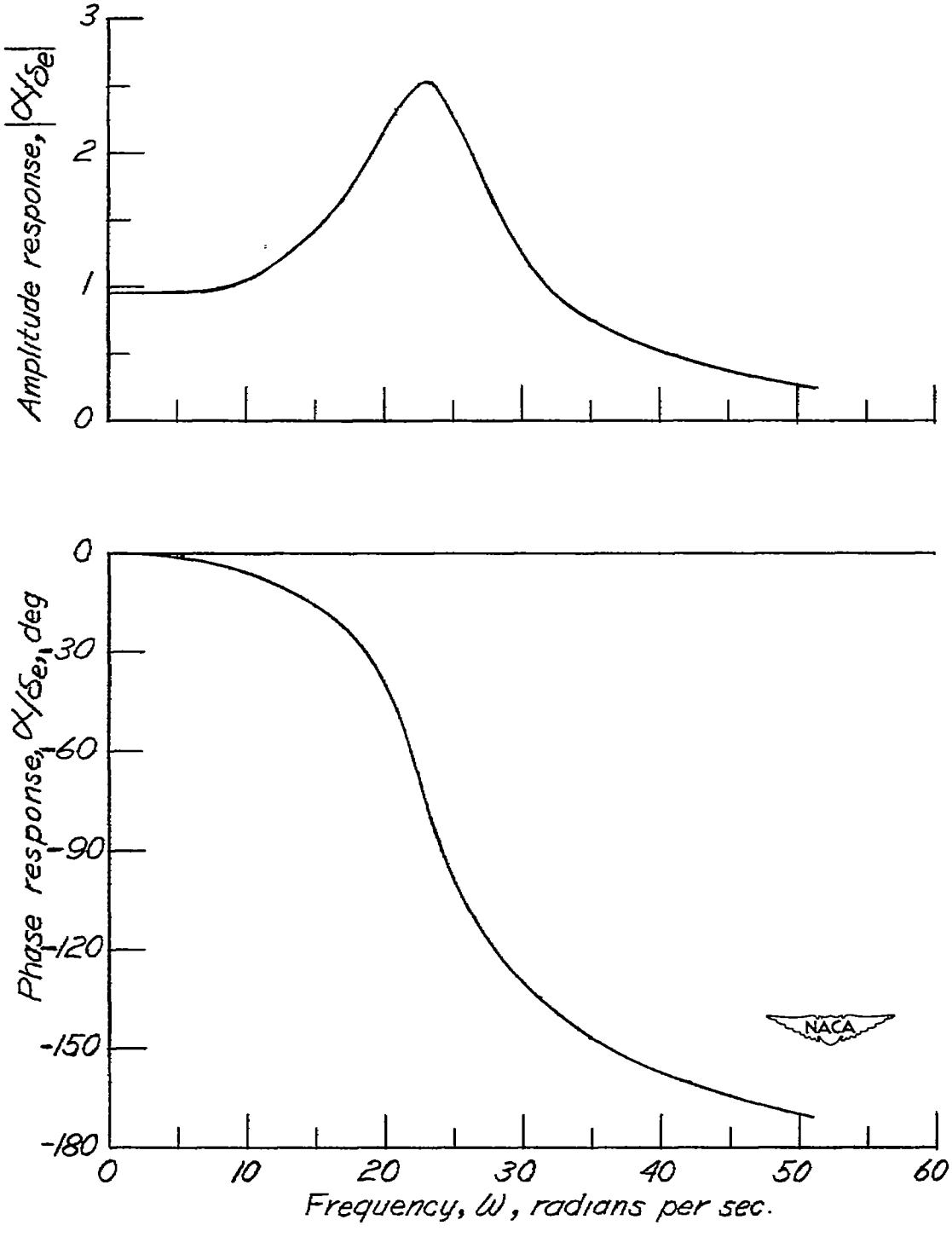

Figure 14.- Typical $\frac{\alpha}{\delta_e}$ frequency response determined from angle-of-attack transient response. Average Mach number, 1.595.

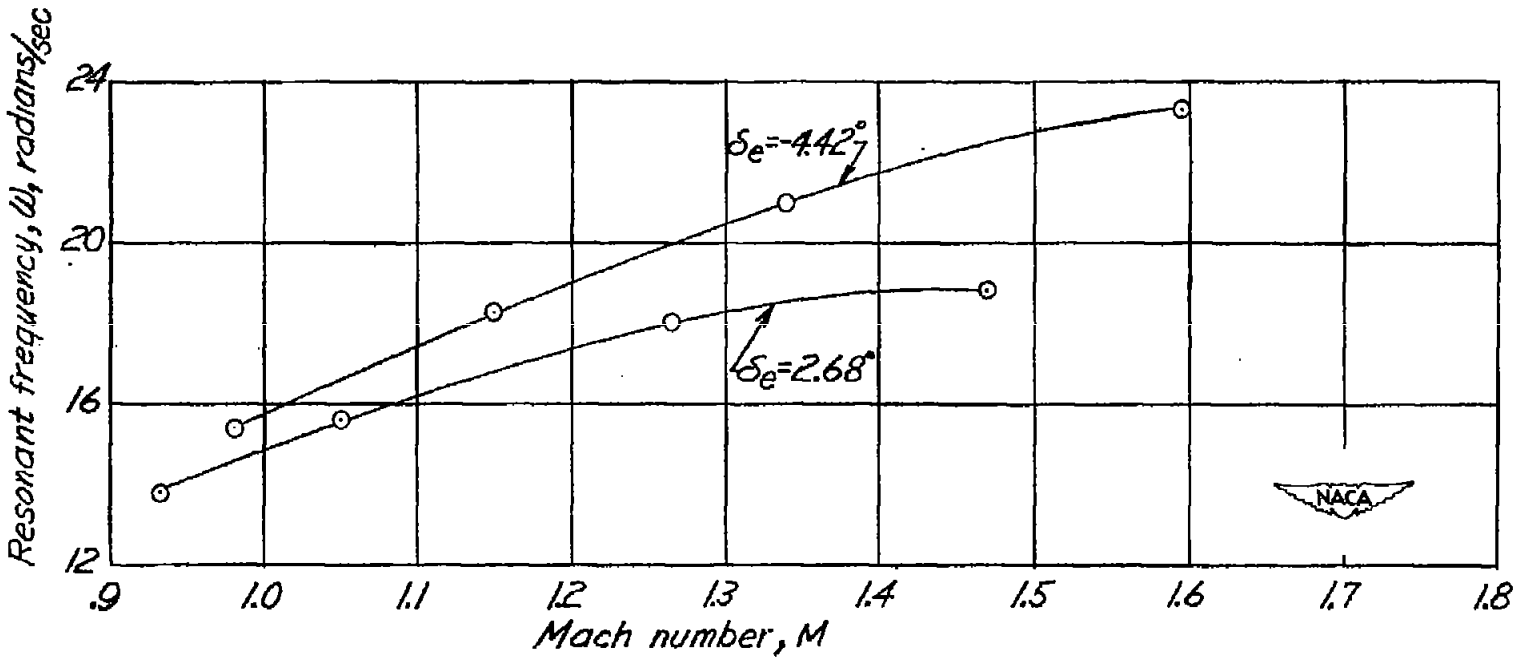

Figure 15.- Resonant or damped natural frequencies of the missile model frequency responses as a function of Mach number.

NACA - Langley Field, Va.